The synthesis of matrices of embedded semiconducting nanowires

Kirk Ziegler,[a] **Kevin M. Ryan,**[a] **Rory Rice,**[a] **Timothy Crowley ,**[a] **Donat Erts,**[b] **Hakan Olin,**[c] **Jenny Patterson,**[d] **Trevor R. Spalding**[a] **Justin D. Holmes**[a] **and M. A. Morris***[a]

[a] *Department. of Chemistry, University College Cork, Cork, Ireland.*
  E-mail: m.morris@ucc.ie; Fax: +353 21 4274097; Tel: +353 21 490 2180
[b] *Insitute of Chemical Physics, University of Latvia, Rainis blvd., 19LV-1586 Riga, Latvia*
[c] *Physics and Engineering Physics, Chalmers University of Technology, SE-41296*
  Göteborg, Sweden
[d] *Intel Ireland, Leixlip, Co., Kildare, Ireland*

In this work we report how single crystal nanowires can be assembled into regular arrays using mesoporous thin films to define the architecture. Mesoporous thin films were prepared by a sol–gel method. These provide films of very regular structure and dimensions. The films produced in this way have almost single crystal like structures and can also exhibit strong epitaxy to the underlying silicon substrate. The films are subjected to a supercritical fluid (SCF) environment in which a precursor is decomposed to yield nanowires of metals, semiconductors or oxides. Using these SCF conditions, pore filling is complete and the products are nanowires which are single crystals and structurally aligned in one direction. The growth mechanism of the nanowires is described and size effects discussed.

Introduction

Moore's Law (the number of transistors on an integrated circuit chip doubles every 18 months), first expressed in the 1960s, has become the basis of the International Technology Roadmap for Silicon and driven progress in the electronics industry for over 20 years.[1] The requirement to maintain the law will require transistor devices on less than 20 nm scale dimensions within only a few years time. Importantly, continued miniaturisation of the complex architectures used in circuitry by conventional lithographic techniques (top-down) will become cost prohibitive.[2] Thus there is a twin requirement to develop *nanoscale* materials within *assembled architectures*. However, in terms of the development of CMOS type devices (and these are expected to dominate developments for at least ten years[3]) the nanotransistors have to be in architectures where they can be electrically contacted and in very high densities at substrate surfaces. This will require periodic nanoscale structures to be prepared of exact dimensionality over macroscopic distances. Workers at Intel have described how practical circuitry may be realised from nanoscale assemblies.[4] The realisation of these structures by chemical means is a very significant challenge. One dimensional (1D) structures, such as nanowires and carbon nanotubes, have enormous potential as building blocks for nanoscale structures as they can function both as devices and as the wires that access them (so overcoming the interconnect problems that are likely to occur. Gargini has described an ideal future transistor based around such a device.[3] Lieber and co-workers have made considerable

progress in the preparation and manipulation of nanowires into useful configurations for nanoscale electronic devices.[5] However, it is difficult to see how circuits with device densities of 10^{10} per chip (in line with expected densities by the end of this decade[6]) can be attained by these methods

The assembly of conducting, semiconducting, magnetic and photonic materials by the filling of ordered porous materials is an attractive means of producing two dimensional arrays of nanowires. Such arrays might allow architectures to be fabricated which might facilitate 'bottom-up' alternatives to conventional (lithography) integrated circuit (IC) processing. However, in order to approach wire dimensions where finite size effects become important (certainly for semiconductors) the dimensions of the pores must be in the mesoporous regime. These dimensions are also those required to process IC technologies beyond the lithographic imposed limitations of Moore's Law. To this effect we have recently demonstrated a supercritical fluid (SCF) inclusion technique to produce silicon and germanium nanowires within the pores of mesoporous silica powders.[7,8] Unlike inclusion of materials within mesopores by other techniques, the SCF method allows essentially 100% filling of the pores. In this way, the materials prepared are effectively the first three dimensional array of nanowires insulated at a finite distance of separation. Discrete transitions observed in the uv-visible absorption and photoluminescent (PL) spectra of the mesoporous silica constrained nanowires suggest that they possess unusual optical properties that could be exploited in a number of applications.[9]

However, in order to progress this work it is necessary that these mesoporous solids be cast as mesoporous thin-films (MTF's). To provide useful alternatives to top-down lithographic methods the films must be mesoscopically ordered over **macroscopic** dimensions, they must have mechanical and adherence consistent with processing and the sizes of the pores must be controllable and reproducible. There have been many efforts to provide unidirectionally ordered MTF's. Frequently this has required slow growth from dilute solutions at the solvent–atmosphere interface.[10] Other techniques rely on electrical or magnetic fields[11] or flow[12] to direct the ordering. More recently, efforts have been made to prepare films from sol–gel precursors where surfactant ordering takes place following rapid solvent evaporation during film drying. Grosso *et al.*[13] and Ogawa *et al.*[14] have been important pioneers of this work. It is apparent that highly ordered films with pore directions defined by substrate anisotropy can be prepared at surfaces.[15] Films formed using these methods typically lack the mechanical and thermal stability necessary to survive the high temperature (800 K) and high pressure (400 bar) required for supercritical fluid deposition. In this work, aluminium containing MTF's (Al-MTF's), templated from neutral triblock copolymer poly(ethylene oxide) (PEO)-poly(propylene oxide) (PPO)-poly (ethylene oxide) (PEO) surfactants, were prepared by simple sol–gel routes. Aluminium incorporation into the silica matrices promotes hydrothermal and mechanical stability. Details of the preparation are described elsewhere.[16]

Experimental

The synthesis of mesoporous aluminosilicate thin-films (Al-MTFs) is based on a modification of the method described by Yoldas for the production of non-porous films.[17] 7 g of a Synperionic triblock copolymer (*e.g.* F127 ($PEO_{106}PPO_{70}PEO_{106}$)) were dissolved in tetraethoxysilane (TEOS) (25 g) and added to a solution of ETOH/(HCl 0.12 M). The resultant solution was stirred at 40 °C for 10 min to prehydrolyse the silica precursor. The solution was cooled in an ice bath prior to the addition of 1 g aluminium *sec*butoxide ($AlOBu^3$). Finally, 2.5 ml of water were added and the solution allowed to condense for 20 h prior to film casting. Polished (110) orientated silicon wafers were cleaned by immersion in nitric acid, washed with water followed by acetone before being ultrasonically treated in triply distilled water prior to spin coating. It was found by detailed X-ray diffraction work that these silicon wafers were slightly off-cut by 0.3° (see below). Ethanol was spincoated at 2000 rpm for 10 s before 30 s of coating in the sol. Cast films were dried at 373 K for 40 min to complete the condensation process and subsequently calcined at 773 K for 1 h to effect template removal. Any residual surfactant was removed completely, as determined by Fourier transform infrared analysis, by placing the calcined films in a concentrated ozone stream for a further 20 min at room temperature.

A supercritical fluid inclusion-phase technique was used to prepare nanowires by deposition within the mesoporous of Al-MTFs. We have already shown that the pores of mesoporous

powders can be completely filled with single crystal nanowires.[7–9] Ordered Al-MTF's were coated with a suitable nanowire precursor (diphenylgermane, copper(II) hexafluoroacetylacetonate, dicobalt octacarbonyl) and placed in a 100 ml high pressure cell under an inert atmosphere. The cell was attached *via* a three-way valve, to a stainless steel reservoir ($\sim$21 ml). A high-pressure pump (Isco Instruments, PA) was used to pump CO_2 through the reservoir in to the reaction cell. The cell was placed in a furnace and for germanium nanowire production was simultaneously heated and pressurised to 500 °C/375 bar for 30 min (or 300 °C/207 bar/30 min for Cu or Co nanowires).

Powder X-ray diffraction (PXRD) data were collected using a Philips Accelerator apparatus equipped with a conventional Cu anode. Incident 0.2 Stoller slits and programmable divergent slits were used. A knife edge held 0.5 mm above the sample was used to limit scattered radiation. Sample zero positions were determined by use of a knife edge and rotation in the X-ray beam. Data was collected at scan rates of about 1° s^{-1}. Accurate Θ and Ω positions were determined relative to a pressed silicon powder sample. AFM characterization (Digital Instruments Dimension 3000 Scanning Probe Microscope), courtesy of Intel Ireland, was performed in tapping mode with silicon cantilevers. SEM data were collected on a JEOL JSM-5510 apparatus. High resolution TEM (HRTEM) data were collected on a JEOL2010F field emission TEM, courtesy of Intel Oregon, with EDX attachment. Data were also collected on an STM-TEM probe at Chalmers. Full details of this are given elsewhere.[18] Typically films were thinned using a focused ion beam such that some gallium ion damage is expected. Brunauer–Emmett–Teller (BET) isotherms at 77 K on a Micrometrics Gemini 2375 volumetric analyser were used for pore size determination using the Barrett–Joyner–Halenda (BJH) model from a 50-point BET surface area plot. Each sample was degassed for 12 h at 573 K prior to a BET measurement.

Results

Mesoporous thin film synthesis

Al-MTFs were prepared by methods detailed elsewhere.[16] These techniques allow films of very high quality and demonstrating mesopore ordering over macroscopic distances. Typical data for a F127 surfactant derived film are detailed here in illustration of the quality of films produced. Typical conventional 2Θ data are provided in Fig. 1. At higher angles there is no sign of broad features assignable to either amorphous materials or poorly structured materials and so only low angle data are shown. The lack of an amorphous feature in the films is probably related to two factors. Firstly,
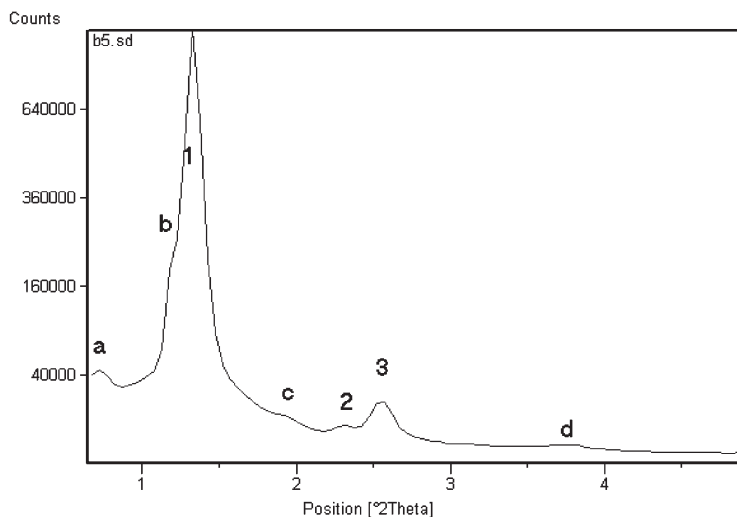
Fig. 1 Typical PXRD pattern of a hexagonally ordered mesoporous thin film at a silicon substrate. Peak assignment is made in the text.

the very high signals seen for the low angle features probably ensure that any low intensity signal is lost in the background noise at these high scan rates. Secondly, strong focussing of the diffraction peaks from very well-ordered films in the Bragg–Brentano geometry can minimise amorphous signals in the presence of strong diffraction features. We believe that these films are amongst the highest quality materials of this type prepared by a simple sol–gel technique to date. They appear to have the same single crystal-like arrangement observed for mesoporous films prepared by very careful substrate preparation and slow film crystallisation processes.[10] Other sol–gel MTF tri-block synthesis methods yield less ordered pore systems after calcination.[13,19,20] The films are certainly the most ordered examples of aluminosilicate films prepared to date although good ordering was achieved by Ogawa *et al.* for films prepared using alkylammmonium chloride surfactants.[14] In all cases described here the films exhibit hexagonal or cubic arrangements of the uniaxial pores. For F127 templated Al-MTFs the PXRD profile exhibits three peaks (1, 2, 3 in the figure) and identified as the (100), (110) and (200) reflections typical of 2D hexagonal pore arrangements. Corresponding *d*-spacings are 6.65, 3.81 and 3.42 nm respectively. The latter two measurements can be compared to values of 3.84 and 3.36 nm ((110) and (200) respectively) calculated using the (100) *d*-spacing. This indicates only low strain in the mesoporous film system. Additional weak diffraction features can also be seen and these are marked a to d in the figure. These are at 0.760, 1.196, 1.957 and 3.755° 2Θ. These correspond to reflections from (1/3,1,0), (1/3,1/2,0), (210) and (300) planes respectively. That these are observed indicates both the very high long range order of the film (resulting in high resolution and peak intensities) and the quality of the data collection. The observation of reflections at greater repeat distances than the (100) reflection may be attributable to the slight strain (as noted above) of the hexagonal lattice observed which results in a larger unit cell. However, they are more likely to be due to experimental conditions discussed below. They are not observed if the film is scraped off and analysed as a powder sample.

The diffractogram shown in Fig. 1 suggests that the pores are aligned parallel to the surface plane. Hillhouse *et al.* have shown that in reflection powder X-ray diffraction studies (as here) from mesoporous films not all of the reflections observed in studies of equivalent powder samples can be observed and that only planes that are parallel to the surface are observed in the usual 2Θ geometry.[21] The observation of a large (100) reflection, (200) and (300) reflections coupled to a relatively low intensity (110) (the (100) to (110) peak intensity ratio is around 350:1) feature suggests that the film is aligned with the (100) plane parallel to the surface. Note that the relative intensity of the (200) to (110) features is about 30 compared to at least intensity expected from powder samples.[22] That weak (110) and the other partial order reflections are observed might suggest that there is either a small misalignment of the film or that small parts of the film are randomly orientated. Both of these explanations are not favoured by the more detailed PXRD data discussed below which suggest that the films have very well aligned pores over the whole of the sample. Instead, we believe that these features are observed because of the low angle experiment and the current instrumentation. The very low angle of incidence ensures that the incident radiation slit image is several mm wide at the sample. This coupled to the high area detector ensures that simple Bragg reflection conditions are not exactly met and otherwise symmetry forbidden reflections can be weakly observed.[10,23]

The alignment of pores is confirmed and analysed further by azimuthal studies. A description of the sample geometry is shown in Fig. 2. Φ is the azimuthal angle, Ω and Θ are the incident and reflected angles to the surface plane respectively and Ψ is the out of plane rotation. The angle Ψ was determined to be zero along a silicon wafer $\langle 110 \rangle$ direction as described below. Normal (in plane) Θ *vs.* 2Θ were data collected as a function of azimuthal angle. The peak intensities of the low angle reflections from the film were normalised to the background intensity at 5°. The results of the azimuthal scans are shown in Fig. 3 from zero to 180° Φ. It can be clearly seen from Fig. 3 that all reflections show strong maxima at 0 and 180°. There are pronounced minima at around 90 and 270° (not shown). These azimuthal dependencies are similar to those observed from films grown by a slow development process.[15] However, the explanation offered by these authors is somewhat different to ours. Miyata and Kuroda suggested that azimuthal dependences could be caused by domain effects within the disordered calcined films.[15] This is not the origin of the effects seen here. No strong grain-like texture was observed by electron microscopy or AFM (see below). Further, the ordering of the calcined film described here is considerably more than those prepared by Miyata and Kuroda where weak intensity, broad (100) reflections were observed without any higher order
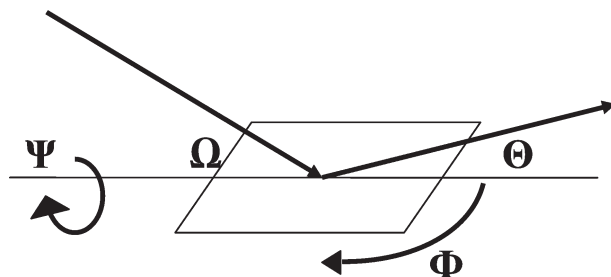
Fig. 2 Schematic of the sample geometry for PXRD studies. Angles are discussed in the text.

features being apparent. Instead, we argue that the azimuthal dependence is related to preferential diffraction of the X-rays when they are perpendicular to the X-ray beam direction. The broadness of the azimuthal dependence arises from the experimental set-up. In this experiment we are scanning along a powder ring by rotation of the sample whilst maintaining the direct alignment of source and detector. Thus, diffracted peaks will remain visible although the intensity difference will vary as a function of $\cos \Psi$ as observed.

The film alignment relative to the substrate was confirmed by carrying out experiments at fixed angles of incidence. These studies provide data equivalent of slices through the 3D diffraction pattern. Importantly, they also allow a film diffraction feature to be studied which would show
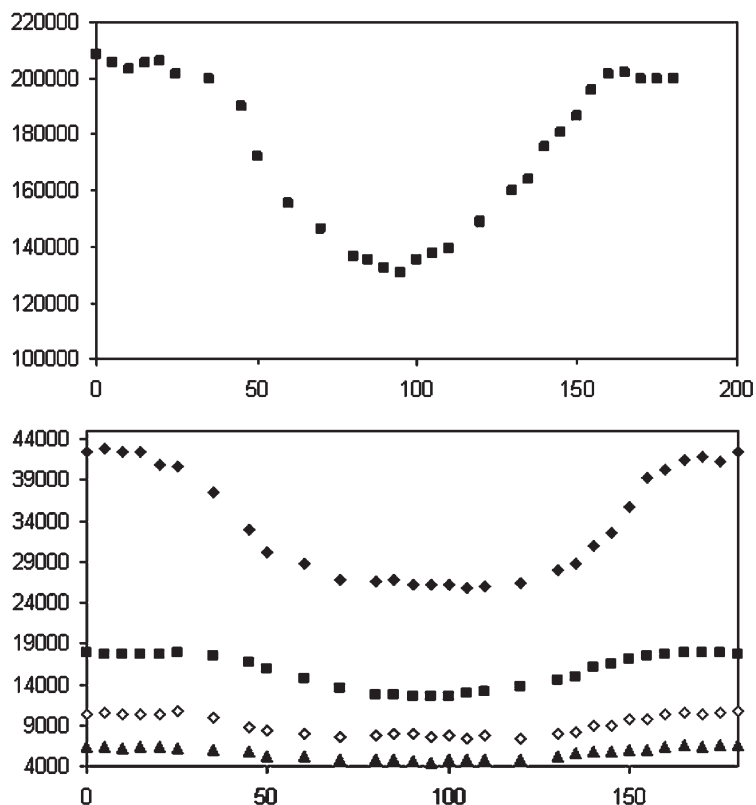
Fig. 3 Azimuthal dependence of the intensity of the PXRD (100) reflection from mesoporous silica films (upper plot). The lower plot shows similar data from the (1/3,1,0) (◆), (200) (■), (210) (◇) and (110) (▲) reflections.

Table 1 Main Bragg reflections observed at $\Omega = 90°$ as function of Φ

Azimuthal angle (Φ)	Bragg reflection
0.00	(511), (440), (531), (620), (533), (444)
18.6	(440)
25.2	(531)
35.2	(440), (531)
45.0	(620), (533)
54.8	(440)
63.6	(440)
70.2	(531)
90.0	(511), (440), (531), (620), (533), (444)

strong azimuthal sensitivity (*i.e.* a non-Bragg diffraction feature. Data were collected to provide information throughout *k*-space but only a limited set of data is reported here. Initially, Ω was set to normal incidence $-90°$ (a range of other angles were used to probe a large part of *k*-space but these are reported elsewhere) and the 2Θ direction scanned from the plane of the sample surface (90°) to 60° above. This is repeated for azimuthal angles between 0 and 180°. At certain azimuthal angles strong Bragg diffraction features from the silicon single crystal substrate are observed. These allow the orientation of the wafer to be determined and $\Psi = 0$ was set at a $\langle 110 \rangle$ direction. Analysis of the peak positions would suggest a small 0.3° misalignment of the sample surface. These data are summarised in Table 1. In all cases the width of the diffraction feature in the azimuthal direction was about 1° Φ. It can be seen that the data are four-fold symmetric as might be expected from a cubic system.

Pore geometry was determined in a similar fashion. At $\Omega = 60°$ a Laue type diffraction feature of the film was observed but only at azimuthal angles of 0 and 180°. Typical data are illustrated in Fig. 4 which shows data collected over 2Θ at $\Omega = 60°$ and $\Phi = 0°$. Bragg reflection peaks from (400), (422) and (511) planes can be seen. There is a very weak feature just resolvable equivalent to a (331) reflection. There is a feature visible at 80.308° 2Θ which is not related to Bragg diffraction. It is also observed from virgin (uncoated) substrates and is clearly due to the silicon substrate. Laue
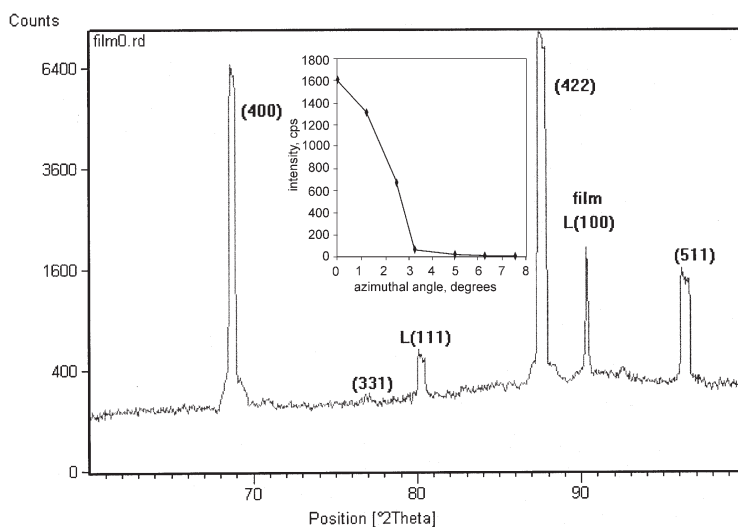
Fig. 4 PXRD pattern recorded with $\Omega = 60$ and $\Phi = 0°$ for film coated Si substrate. Peaks are indexed as described in text; L indicates a Laue diffraction feature. The inset shows the intensity of the Al-MTF L(100) feature as a function of azimuthal angle.

diffraction (diffraction condition is $d(\cos\Omega - \cos\Theta) = n\lambda$) can occur from planes within the bulk. The feature at 80.308° 2Θ thus appears at a position exactly described by a (111) reflection from a substrate (211) plane. One feature observed in the data at 90.366° 2Θ is only observed from mesoporous film coated samples. For Laue conditions diffraction from large d-spacing materials can only be observed at conditions where Ω and Θ are around the same value. Again, but assuming reflection from a hexagonal mesoporous structured film (520) plane, the d-spacing can be calculated as 6.67 nm and is indexed as a (100) reflection from the film. It is in very close agreement with the lattice parameter measured from standard Θ–2Θ data above. This Laue diffraction feature is narrow (in Φ) with a half full width half maximum at 2.5° (Fig. 4). The data clearly indicate that the pores lie in directions along a substrate (110) plane (since the $\langle 110 \rangle$ direction is normal to these planes). This observation would suggest an epitaxial relationship of the film to the substrate. Silicon has a known lattice parameter of 0.543 nm equivalent to a (110) d-spacing of 0.384 nm. Within experimental error this is precisely ten times less than the mesoporous film (110) d-spacing and supports the epitaxial relationship suggested here. The arrangement at the surface was confirmed by AFM studies. Fig. 5 shows a schematic of the arrangement and an AFM image collected from the sample and substrate. The AFM clearly shows a slight rumpling of the film surface indicative of the pore arrangement. Finally, comment should be made on the shape of the diffraction features observed from the substrate. As can be seen in Fig. 5, these are actually made up of two individual features with 'flat' tops. This was typical of data collected at any Ω or Φ angle from the film coated samples. Peaks from uncoated samples had more normal Gaussian shapes. The doublets observed are not Kα_1 and Kα_2. Instead we believe that these are small changes in peak position observed because of X-ray refraction through the film.

Not all films prepared by these methods produce horizontally aligned pores. Particular substrate–surfactant combinations can produce pores which are vertically aligned relative to the
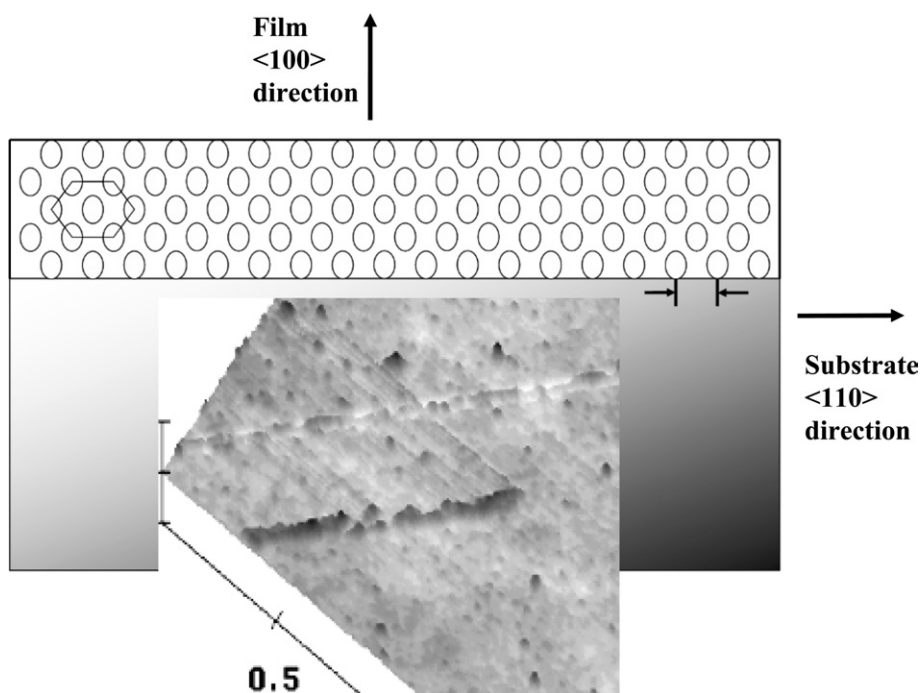
Fig. 5 Schematic showing the arrangement of pores at the surface of the silicon wafer. The crystallographic directions are marked. The distance between pores at the surface marked with arrows = 10 Si(110) lattice spacings. The inset shows an AFM image of the surface of a mesoporous film coated wafer. The horizontal scale bar is 0.5 μm. The vertical scale bar is 10 nm. The rumpling caused by the pores runs parallel to the scale bar. Two scratches (for strength testing) running perpendicular to the pore direction can also be seen. The rumpling of the film is around 0.2 nm.

substrate plane. Fig. 6 illustrates PXRD data from an Al-MTF prepared as above using a P123 ($PEO_{20}PPO_{69}PEO_{20}$) surfactant. The inplane scan taken at $\Psi = \Phi = 0$ (*i.e.* with the plane of the surface in normal geometry) shows no sign of mesoporosity with no low angle features visible. The low angle intensity observed is simply the tail of the straight through X-ray beam. This suggests that pores are perpendicular to the sample surface.[21] If the sample is moved through 90° Ψ so that the plane of the surface is parallel to the plane of the X-rays and a Θ–2Θ scan taken (Fig. 6 also) additional features become apparent due to diffraction from the planes of pores in the correct direction to allow Bragg diffraction. With this apparatus in this geometry there is very high background and the peaks are not clearly defined at these very low angles. As an inset to the data there is a background subtracted profile shown. This shows the presence of three features at 2Θ angles equivalent to *d*-spacings of 3.933, 2.979, 2.463 nm. The relationship between these *d*-spacings *i.e.* 3.933/2.979 = 1.32 and 3.933/2.463 = 1.597 can be compared to similar values of measured for the *d*-spacing values of the planes: (220)/(321) and (220)/(420) for a cubic structured mesoporous material.[24] The microscopy data described below indicate that these films do not have a gyroid (*Ia3d*) type structure. Further, the PXRD intensity pattern is not reminiscent of this type of structure. Instead it is more likely that the film has a structure similar to the centred rectangular arrangements observed by Grosso *et al.*[25] However, it is clear that there is a cubic mesoporous
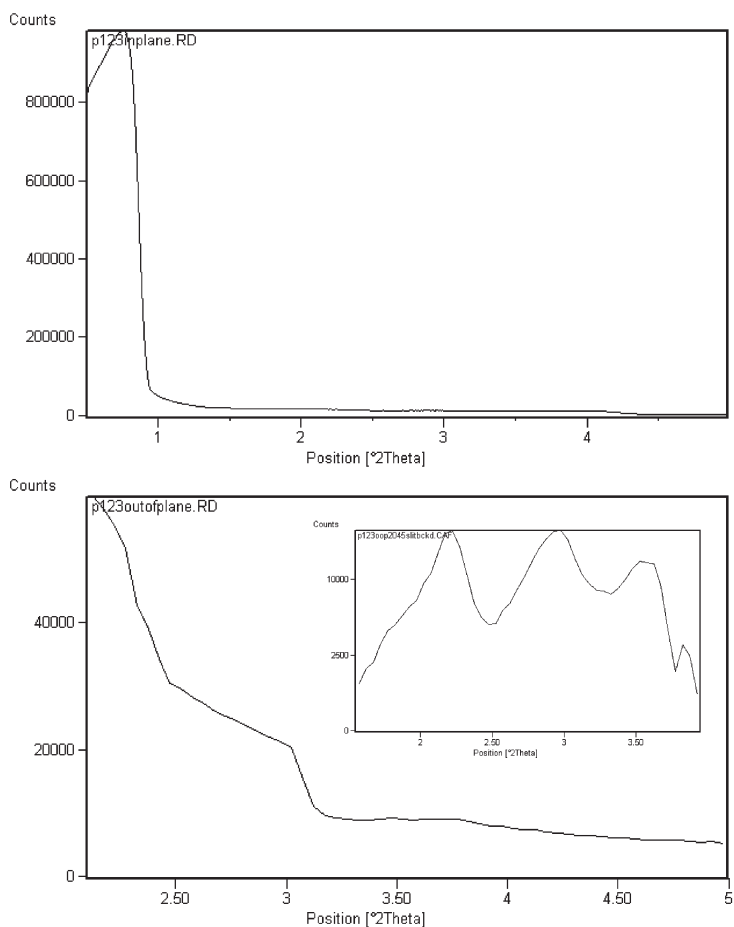
Fig. 6 Upper plot shows PXRD data taken from P123 derived Al-MTF with the sample in the normal diffraction plane. The lower plot shows data from the same sample held orthogonal to the normal plane ($\Psi = 0$). The inset shows data after a background subtraction.

structure with a vertical alignment of pores. Since both films were prepared in the same way, it would appear from the results presented here that substrate structure has a profound effect on determining pore alignment.

Nanowire formation by inclusion of materials within the mesopores

The advantages of SCF conditions in preparation of nanowires by inclusion into mesopores have been discussed previously.[7,8,27] Briefly, SCF conditions allow high mass transport rates so that, in optimum conditions, particle growth rates can exceed nucleation rates. Further, the use of pressure and temperature can be used to select crystallite orientation.[26] Importantly, SCF conditions allow surface tensions to be minimised allowing highly effective pore filling. Because of these factors the growth mode of wires within the mesopores that we have observed thus far is radial. Fig. 7 shows data illustrating this growth mechanism for the growth of Co nanowires in P85 ($EO_{26}PO_{39}EO_{26}$) surfactant templated mesoporous silica. Co nanowires were prepared at various concentrations of precursor (to the free pore volume). The AFM image shows the image of the surface after over-filling with cobalt. The wires within the pores have begun to nucleate into larger particles but the hexagonal ordering of the pore system can still be seen. Under-filling of pores does not produce particles but rather it produces nanotubes in which the metal 'lines' the pores of the pore. This is illustrated by data recorded for Fe_3O_4 nanowire systems. The SCF technique allows manipulation of the crystal structure of the wires through control of pressure and temperature. PXRD of nanowires in the pores can easily separate these phases (also in Fig. 7). Table 2 shows the results of structural manipulation. The ability to manipulate the crystal structure of the Co nanowires is of
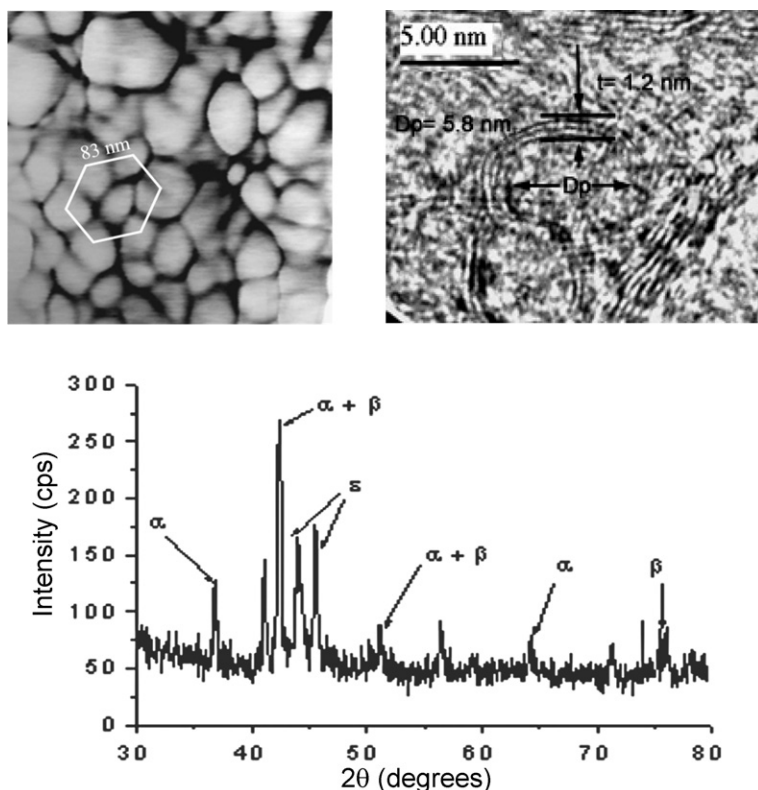
Fig. 7 Upper plots are an AFM image (left) of an over-filled sample of Co nanowires. The wires are beginning to nucleate and grow as 3D particles at the surface but the hexagonal arrangement of underlying pores can still be seen. Right is a TEM image of a nanotube of Co formed by partial filling. The lower image is a PXRD of Co nanowires within the mesoporous matrix illustrating the formation of three Co phases.

Table 2 The effect of SCF reaction conditions on the crystal structure of cobalt nanowires synthesized in mesoporous silica. α, β, and ε are the hexagonal, cubic and metastable cubic phases respectively

Pressure/bar	Temp/°C	Crystal phase (%)			Fluid density/g cm^{-3}
		α	β	ε	
138	300 °C	42.9	15.9	41.2	0.132
276	325 °C	5.7	9.0	85.3	0.247
276	350 °C	7.4	15.5	77.1	0.234
276	477 °C	28	31.7	40.3	0.187
276	500 °C	0	100	0	0.180
345	400 °C	76.5	23.5	0	0.261
345	500 °C	0	100	0	0.221

considerable importance due to the strong correlation between the crystal structure and the magnetic properties of bulk Co. The anisotropic high magnetic coercivity of the HCP phase is the preferred structure for permanent magnetic applications (recording media); while the more symmetric low coercivity FCC phase is more useful for soft magnetic applications.[28] All of the wires produced here retain the ferromagnetic characteristics of bulk materials.

Further evidence for the radial growth mode is illustrated in data following Co nanowire insertion (Fig. 8). The first data shown is a plot of pore size measured by BET (N_2 adsorption) following exposure of P85 ($EO_{26}PO_{39}EO_{26}$) surfactant templated mesoporous silica to various amounts of copper precursor (as above) and subsequent SCF reaction. The measured progression of pore size follows the trend expected if all of the copper is used to evenly coat the pores of the material. The agreement of data to theory is excellent for simple particle filling one would expect more sudden trends as pores would block at relatively low loadings. A schematic of the radial growth mechanism is also shown. TEM also shows that smooth nanotubes are formed and intermediate loadings. The tube-like nature of the copper is clearly demonstrated after the silica matrix had been dissolved by an acid etch. The progressive nature of the growth results in gradual changes in the physical properties of these materials. If PXRD is used to estimate the unit-cell parameter (FCC structure) of copper as a function of loading it can be seen (Fig. 8) that this continually decreases until the bulk value of 0.3615 nm is reached. This is important. Theory suggests that isolated nanowires demonstrate lattice contraction because of surface tension effects. By containment within the pores these surface tension effects are minimised and quantum confinement effects result in lattice expansion.[8]

Whilst copper and cobalt nanowire arrays may have important applications in the area of interconnects and magnetics our greatest interest has been in the design of these embedded matrices to provide means to assemble nanowires arrays of semiconductors.[27] In order to produce arrays for potential use in semiconductor applications the Al-MTFs have to be of very high quality *i.e.* crack-free, well-adhered *etc.* Fig. 9 shows typical electron microscope data (on-top and cross-section SEM images) of P85 derived Al-MTF. It can be seen that the Al-MTFs produced in this work are extremely uniform. During microtoning for electron microscopy imaging no delamination of the films occurs. This indicates strong adhesion and all of the films prepared here survive Scotch Tape and scratch tests. The films show no degradation in quality during SCF treatment.

The P85 films also show a similar vertical alignment of pores (as discussed above) for P123 samples. This is confirmed by analysis of the material by TEM. Data is shown in Fig. 10 from a fragment of the film after germanium nanowire growth. The perpendicular nanowires can be clearly seen. This complex architecture was confirmed by 2D elemental mapping using high spatial resolution EDX.[27] In the figure individual EDAX spectra are shown confirming the presence of Ge from only the dark regions of the sample (nanowires). BET analysis revealed the extent of pore filling. Prior to the Ge-SCF reaction the material was characterised by a surface area of 600 m^2 g^{-1} and a pore size of 5.0 nm. Following pore filling of this film the surface area reduced to 5 m^2 g^{-1} and a pore diameter reduction to 0 nm. Further evidence for nanowire inclusion was provided by high angle X-ray diffraction characterization of germanium nanowires within the pores. The ⟨111⟩ and ⟨100⟩ lattice planes of metallic germanium were evident (data not shown), with lattice
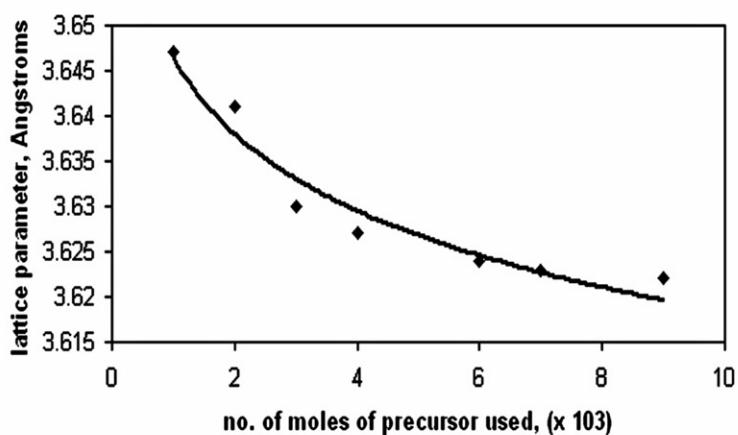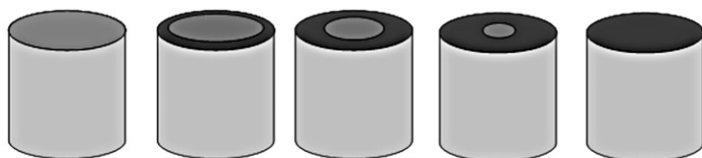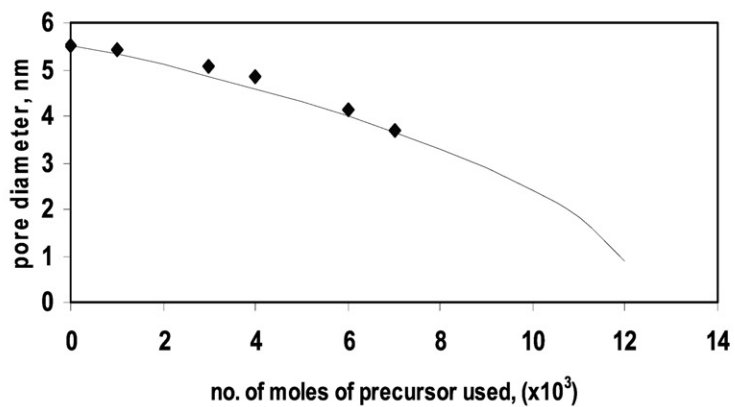
Fig. 8 Upper plot shows the measured (data points) variation of pore size against the amount of copper precursor used during SCF filling of a mesoporous sample. The solid line is the theoretical variation assuming radial growth. The mechanism is illustrated below. Also shown (centre) is a TEM image of copper nanotubes (partial filling) after solution of the matrix (image is 120 nm across). The bottom figure plots the variation in the Cu FCC lattice parameter as function of loading.
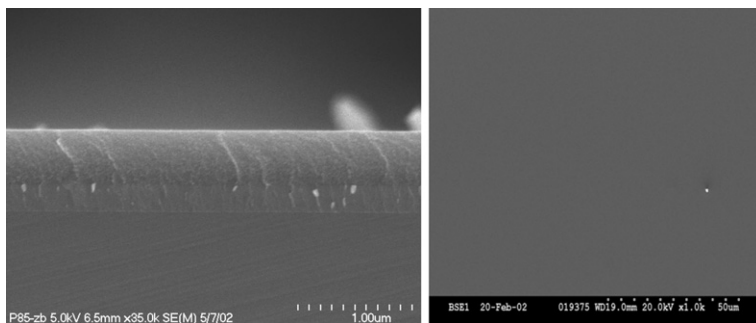
Fig. 9 Upper left and right show SEM x-section and top view of a P85 Al-MTF. These illustrate the crack-free nature of the films.

parameters mirroring mesopore dimensions similar to that previously reported for nanowires constrained within mesoporous powders.[7]

Very high resolution TEM was used to verify the single crystal nature of the nanowires produced by the SCF method. To facilitate ultra-high packing densities, oligomeric polyethylene oxide ($C_{12}EO_{23}$ (Brij35)) templated Al-MTFs were used as hosts and these exhibited pore sizes of around 2 nm (BET) with pore wall thicknesses of around 1 nm (PXRD). Fig. 11 shows a high resolution SEM image of the film. This image only confirms the uniform nature of the film and wires can not be resolved at this resolution. Focused ion beam (FIB) etching was used to reduce the sample to very thin cross-sections to facilitate 200 KV TEM imaging. Magnification reveals the presence of parallel nanowires within the material. High resolution TEM further shows the ordered arrangement of wires. In the lower figure the white arrows show areas where no atomic detail is observed and this can be assigned to the mesoporous walls. In between these areas, the clear presence of well defined atomic planes is evident. These are quite unexpected of the amorphous aluminosilicate present in the mesoporous matrix—high angle PXRD studies do not indicate any sign of crystallisation of the Al-MTF matrix. These single crystal arrangements of atomic planes can be assigned to the presence of germanium nanowires.

It is difficult to analyse these data in detail. The image represents a slice through the films several wires deep and a number of individual wires are sampled. Since the wires are probably rotated to
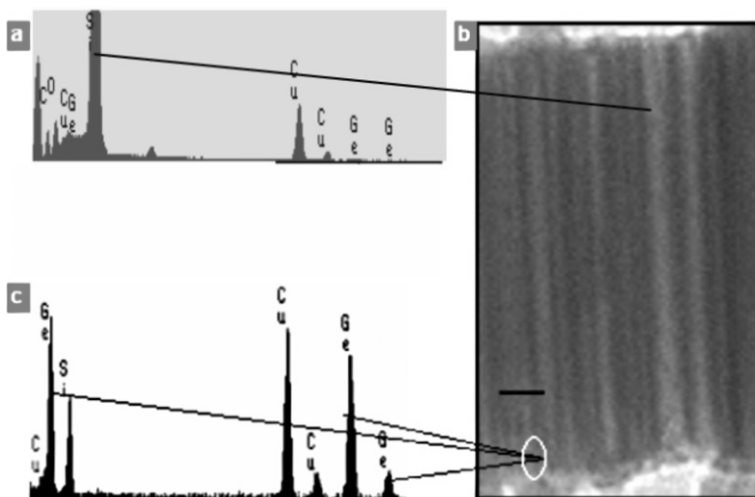
Fig. 10 TEM/EDAX analysis of film described in Fig. 9 after filling with germanium to form nanowires. The EDAX is taken from dark areas (nanowires) and light areas pore wall). Only dark areas show the presence of Ge; Si is observed because of the host matrix. Scale bar is 20 nm.
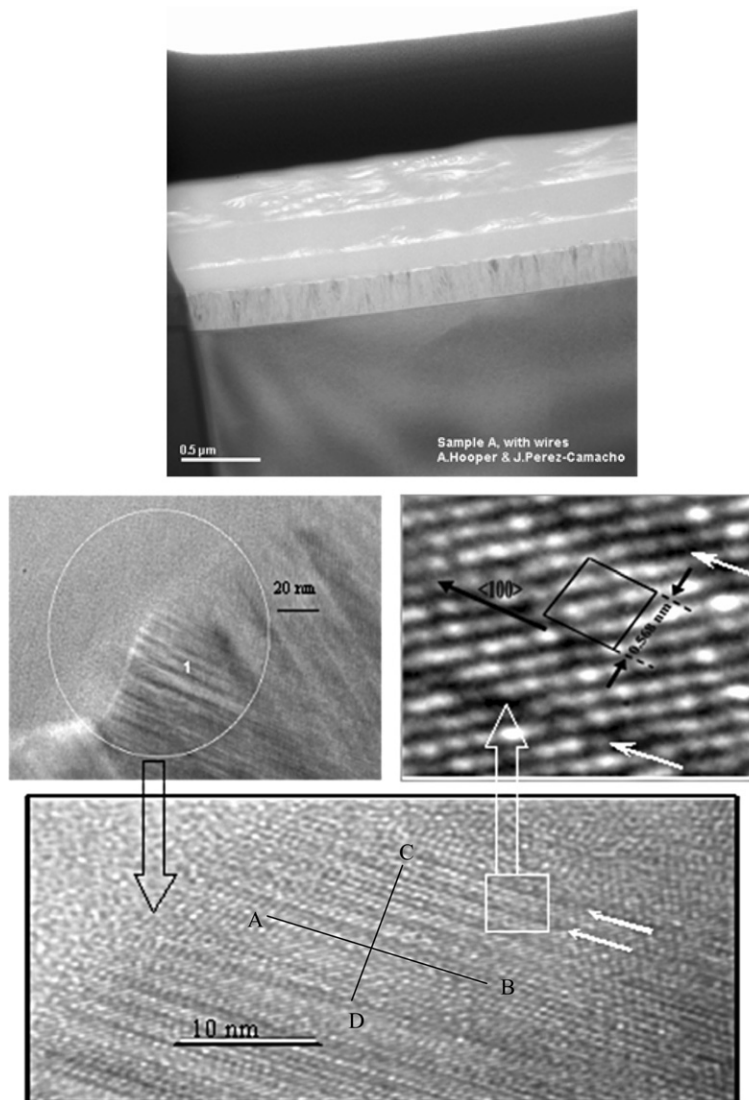
Fig. 11 The topmost image shows a SEM image of a Brij35 derived film. The lower plots show increasing magnification of an area of the Al-MTF by TEM. Further detail given in text.

one another the pattern is extremely complex. However, it can be seen in the figure that the wires have the same crystal orientation. Using intensity data collected along the wires (marked A and B), Fourier analysis indicates strong correlation at a distance of 0.568 nm. Similar analysis in the direction C and D, across the wires gives strong correlations at 0.568, 2.12 and 3.25 nm. The values measured of 0.568 nm almost exactly agrees with that of crystalline germanium at 0.56576 nm reported in the literature[29] and have been used to sketch a 'unit cell'. Whilst this analysis is not complete it is clear that the wires are orientated in the $\langle 100 \rangle$ direction as indicated in the Fig. 11. It can be seen that the nanowires are also free of large defects such as edge and screw dislocations or voids. This is in sharp contrast to the work thus far published on pore-filling of mesoporous materials and strongly indicates the unique ability of SCF techniques to fill these nanostructured matrices compared to more conventional methods. The correlations at 2.12 and 3.25 nm are assigned to the width of the nanowire and a nanowire plus wall width respectively. The values of

2.12 and 1.13 nm are in very good agreement with the pore diameter and wall thickness found by BET and PXRD. It is believed that these data represent the first images of a regular array of nm dimensioned single crystal nanowires constrained within a mesoporous dielectric thin film.

Discussion and conclusions

It is our opinion that many authors grossly underestimate the challenge of fabricating practical (and more importantly commercially viable and processable) devices from even the most elegant of self-assembled architectures. One must firstly consider the considerable spatial accuracy needed to prepare devices. If template structures, such as those used here, are to be hosts for individual nanodevices the dimensions have to be very accurately maintained. At some point it will be necessary to contact these systems with a secondary tool (be it chemical or physical) to define electrical contact. The accuracy required to predict positions of wires over a 30 cm wafer are extraordinary. To approach the required accuracy it will be necessary to have a well-defined epitaxial relationship between the template host and the substrate. Work carried out here and elsewhere is crucial in determining if these techniques will ever be practical. It may be necessary to interface conventional photolithography with these chemical methods so that groups of nano-particles can be used as the devices and the improvement in performance arises from the unique physical properties of 1D nanostructures.

Further, questions remain as to the practicalities of moving individual devices ever closer to increase densities. Very little is foreseen as to overcome the resistive–capacitance coupling (RC coupling) between devices or interconnects over such short distances. Currently, manufacturers are using the metal (copper) with the lowest electrical resistance (silver is slightly better but is very difficult to process) and materials with dielectric constants lower than two remain untried.[1,3,4] However, no matter how severe the challenges are, methods for the possible bottom up fabrication of devices must be developed if the limitations of lithography are to be avoided.[2]

For these reasons it is necessary to use nanoscale particles and their assemblies to define materials with beneficial physical properties (*i.e.* resulting from 1D quantum confinement) as well as being in highly defined structural arrangements. An example would be to define interconnect wires (essentially vias) where electron transport is ballistic rather than ohmic and so reduce resistances and RC effects. We believe that 1D nanowires afford the opportunity to 'design' such properties. Further, by restriction within the mesoporous network it becomes possible to specify an effective particle diameter over a very narrow size range allowing uniform performance to be exhibited by every particle or eventually real device.

Size dependent properties of nanowires are shown in Fig. 12. The first part of the figure shows the normalised photoluminescence (PL) spectra for Ge nanowires constrained within Al-MTFs of 2, 4 and 5 nm pore sizes. These matrices were templated from Brij35, P85 and P123 surfactants respectively. Quartz substrates were used in these measurements for optical transparency. A well-defined shift in energy of the PL emission to higher energies can be observed as the Ge nanowire diameter is reduced. PL is observed in the blue region −2.64 eV (5 nm nanowires), 2.75 eV (4 nm) and 3.01 eV (2 nm). The observed peak positions fit favourably to the energy of the lowest direct $1s_e \rightarrow 1s_h$ transition calculated from theoretical data of quantum confinement in nanocrystals and wires.[30] A broad shoulder can be seen in the data recorded from P85 and Brij35 constrained nanowires. This shift may be due to Si–O–Ge bonding at the pore wall–nanowire interface. Similar features were observed in germanium oxygen deficient carriers or neutral oxygen monovacancies in germanium doped silica films.[31] The data clearly indicate that control of wire diameters by inclusion within pores can be used to define properties.

Finally, we address the problems of contacting these nanowires in order to characterise them. Fig. 12 also shows illustrative data. In this work silicon nanowires were contacted by two AFM tips to provide current–voltage (*IV*) data. Although one wire appears to show ballistic type electron transport, an almost identical wire shows ohmic transport. Differences most probably result from contact problems between the tip and the wire as thin native oxide is likely to coat the wires. There is a real need for work to be carried out in defining methods for electrical (and optical) characterisation of these kinds of architectures if these are to provide a useful means of generating nanoscale electrical circuitry.
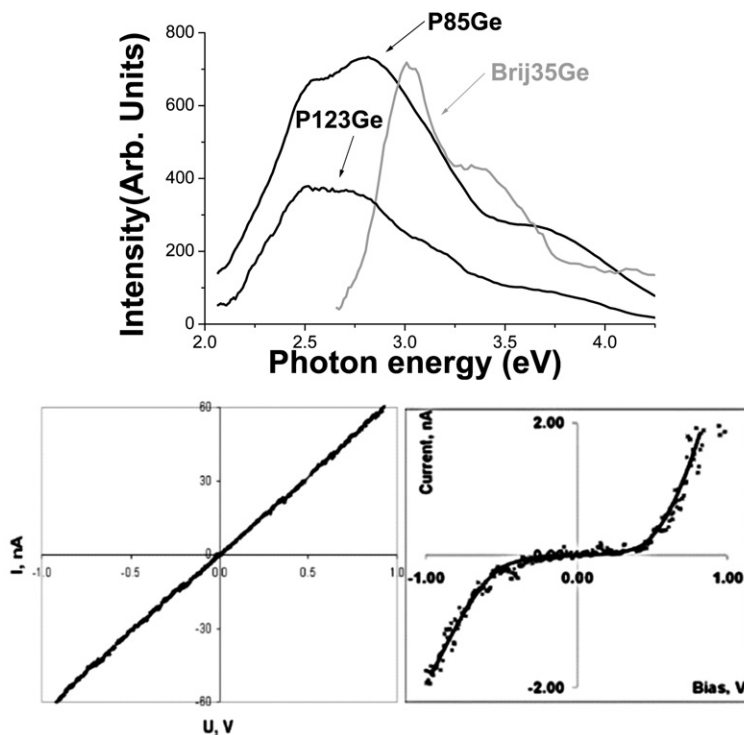
Fig. 12 Upper image shows uv-PL emission spectra of germanium nanowires within a several mesoporous Al-MTFs (excitation energy 1.92 eV). The lower plots show two current–bias voltage (*IV*) plots for silicon wires measured using two AFM tips positioned along the wire.

In conclusion, ultra high density parallel arrays of high purity germanium nanowires were synthesized at silicon wafer substrates. The synthesis of the Al-MTF host and the subsequent nanowire inclusion method may be applicable to future high device density integrated circuit processing. In particular, the high diffusivity of supercritical CO_2 enables rapid transport of germanium precursor into the porous matrix. The very high growth rates favour the production of nanowires of controlled structure in single crystal form. The use of the mesoporous matrix allows the aspect ratio, and orientation of the wires to be controlled. This facilitates strict control of the optical properties of the nanowires. The technology used here could be extended to ultimately prepare perpendicular arrays of 2 nm wires insulated by 1 nm walls and packing densities of 1×10^{12} wires cm^{-2}. This would, theoretically at least, allow Moore's law to be extended for the next 20 years. However, the practicality of such arrays is not certain and parallel progress in many areas of materials and semiconductor science are required to advantage such high densities.

Acknowledgements

References

1 ITRS Roadmap, *Process Integration, Devices and Structures and Emerging Devices Section*, 2001 edition, http://public.itrs.net.
2 D. Maydan, *Mater. Sci. Eng., A*, 2001, **302**, 1.

3   P. Gargini, President ITRS, 2002 ITRS Update, Tokyo International Forum, Tokyo, 1992.
4   *Intel Technol. J.*, 2002, **6**, 42.
5   See for example Y. Cui and C. M. Lieber, *Science*, 2001, **291**, 851; Y. Cui, X. Duan, J. Hu and C. M. Lieber, *J. Phys. Chem. B*, 2000, 104.
6   T. Thurn-Albrecht, J. Schotter, G. A. Kastle, N. Emley, T. Shibauchi, L. Krusin-Elbaum, K. Guarini, C. T. Black, M. T. Tuominen and T. P. Russell, *Science 200*, **290**, 126.
7   N. R. B. Coleman, M. A. Morris, T. R. Spalding and J. D. Holmes, *J. Am. Chem. Soc.*, 2001, **123**, 187; N. R. Coleman, N. O'Sullivan, K. M. Ryan, J. D. Holmes, T. R. Spalding and M. A. Morris, *J. Am. Chem. Soc.*, 2001, **123**, 7010.
8   N. R. B. Coleman, K. M. Ryan, T. R. Spalding, J. D. Holmes and M. A. Morris, *Chem. Phys. Lett.*, 2001, **343**, 1.
9   D. M. Lyons, K. M. Ryan, M. A. Morris and J. D. Holmes, *Nano Lett.*, 2002, **2**, 811.
10 H. Miyata, T. Noma, M. Watanabe and K. Kuroda, *Chem. Mater.*, 2002, **14**, 766.
11 S. H. Tolbert, A. Firouzi, G. D. Stucky and B. Chmelka, *Science*, 1997, **278**, 264.
12 H. W. Hillhouse, J. W. Egmond and M. Tsapatsis, *Langmuir*, 1999, **15**, 4544.
13 D. Grosso, A. R. Balkenende, P.-A. Albouy, A. Ayral, H. Amenitsch and F. Babonneau, *Chem. Mater.*, 2001, **13**, 1848.
14 M. Ogawa, K. Kuroda and J.-I. Mori, *Langmuir*, 2002, **18**, 744.
15 H. Miyata and K. Kuroda, *J. Am. Chem. Soc.*, 1999, **121**, 7618.
16 M. A. Morris, K. M. Ryan, J. D. Holmes and W. Lawton, US Patent, Filed December 2002.
17 B. Yoldas, *J. Non-Cryst. Solids*, 1984, **63**, 150.
18 K. Ziegler, J. D. Holmes, D. Erts, H. Olin and M. A. Morris, *Nat. Mater.*, submitted.
19 T. Yamada, K. Asai, A. Endo, H. S. Zhou and I. Honna, *J. Mater. Sci. Lett.*, 2000, **19**, 2167.
20 G.-Su. Park, C.-W. Ahn and M.-W. Kim, *J. Am. Ceram. Soc.*, 2002, **85**, 2542.
21 H. W. Hillhouse, J. W. van Egmond, M. Tsapatsis, J. C. Hanson and J. Z. Larese, *Microporous Mesoporous Mater.*, 2001, **44–45**, 639.
22 K. M. Ryan, N. R. B. Coleman, D. M. Lyons, M. A. Morris, D. C. Steytler, R. K. Heenan and J. D. Holmes, *Langmuir*, 2002, **18**, 4996.
23 T. Noma, H. Miyata, K. Takada and A. Iida, *Nucl. Instrum. Methods*, 2001, **A467**, 1021.
24 R. Schmidt, M. Stocker, D. Akporiaye, E. Heggelund Torstad and A. Olsen, *Microporous Mesoporous Mater.*, 1995, **5**, 1.
25 D. Grosso, A. R. Balkenende, P. A. Albouy, A. A. Ayral, H. Amenitsch and F. Babonneau, *Chem. Mater.*, 2001, **13**, 1848.
26 J. D. Holmes, K. P. Johnston, R. C. Doty and B. A. Korgel, *Science*, 2000, **287**, 1471.
27 K. M. Ryan, D. Erts, H. Olin, M. A. Morris and J. D. Holmes, *J. Am. Chem. Soc.*, 2003, to be published.
28 S. Ram, *Acta. Mater.*, 2001, **49**, 2297 and references therein.
29 G. Swanson and K. Tatge, *Natl. Bur. Stand. (U.S.)*, 1951, **Circ. 539I**, 18.
30 See for example Y. Kayanuma, *Phys. Rev. B*, 1988, **38**, 9797; L. E. Brus, *J. Chem. Phys.*, 1984, **80**, 4403.
31 D. P. Poulious, J. P. Spoonhower and N. P. Bigelow, *J. Luminesc.*, 2003, **101**, 23.